Received: 17 January 2024 | Accepted: 18 June 2024

DOI: 10.1111/eos.13006

ORIGINAL ARTICLE

European Journal of Oral Sciences | NOF Scandinavian Division IADR | WILEY

Contribution of initial lymphatics to oral wound healing after tooth extraction

Anca Virtej[1,2,3,4] | **Larissa Marti**[1] | **Marek Wagner**[1,5] | **Helge Wiig**[1] | **Ying Xue**[2,4] | **Athanasia Bletsa**[2,6] | **Ellen Berggreen**[1]

[1]Department of Biomedicine, University of Bergen, Bergen, Norway

[2]Department of Clinical Dentistry, University of Bergen, Bergen, Norway

[3]Department of Oral Surgery, Haukeland University Hospital, Bergen, Norway

[4]Department of Clinical Dentistry, The Arctic University of Tromsø, Faculty of Health Sciences, Tromsø, Norway

[5]Łukasiewicz Research Network - PORT Polish Center for Technology Development, Cancer Biomarkers Research Group, Wroclaw, Poland

[6]Oral Centre of Expertise in Western Norway, Bergen, Norway

Correspondence
Anca Virtej, Department of Clinical Dentistry, Faculty of Health Sciences, UiT The Arctic University of Norway, Hansine Hansens Veg 86, 9019 Tromsø, Norway.
Email: Anca.virtej@uit.no

Funding information
HelseVest, Grant/Award Number: HV F-11508; University of Bergen

Abstract

Lymphatics are involved in the resolution of inflammation and wound healing, but their role in the oral wound healing process after tooth extraction has never been investigated. We therefore sought to evaluate the healing process following the extraction of maxillary molars in two transgenic mouse models: K14-VEGFR3-Ig mice, which lack initial mucosal lymphatic vessels, and K14-VEGFC mice, which have hyperplastic mucosal lymphatics. Maxillary molars were extracted from both transgenic mouse types and their corresponding wild-type (WT) controls. Mucosal and alveolar bone healing were evaluated. A delayed epithelialization and bone regeneration were observed in K14-VEGFR3-Ig mice compared with their WT littermates. The hampered wound closure was accompanied by decreased levels of epidermal growth factor (EGF) and persistent inflammation, characterized by infiltrates of immune cells and elevated levels of pro-inflammatory markers in the wounds. Hyperplastic mucosal lymphatics did not enhance the healing process after tooth extraction in K14-VEGFC mice. The findings indicate that initial mucosal lymphatics play a major role in the initial phase of the oral wound healing process.

KEYWORDS
bone regeneration, epidermal growth factor, inflammation, lymphatic vessels, transgenic mice

INTRODUCTION

When a tissue is damaged, specialized cells sense and remove pathogens and manage to restore the function at the injured site in a series of finely tuned sequences [1]. A hemostatic phase commences with blood clot formation, paralleled by the inflammatory phase and in the end, new tissue is formed and remodeled during the proliferation phase, restoring the epithelial barrier function [2]. Blood vessel formation (angiogenesis) is an essential factor in recruiting immune cells, including polymorphonuclear cells (PMNs) and monocytes, which infiltrate the newly formed wound matrix [3]. By killing bacteria, neutrophils clean the wound site before themselves being removed by professional phagocytes such as macrophages, which subsequently take over the wound healing process [4]. Their plasticity, which is modulated by cytokines and growth factors, gives them the ability to promote or resolve inflammation [5]. Macrophages also initiate collagen synthesis and are involved in endothelial cell and fibroblast differentiation. During the development of

granulation tissue, keratinocytes proliferate and migrate across the wound surface [6]. As such, the wound is prepared for tissue regrowth, which occurs during the stages of proliferation and remodeling [7].

In addition to blood vessel formation, adequate growth of lymphatic capillaries from the wound edge is essential during the normal wound healing response [8]. Lymphatics are associated with chemokine signaling, formation of granulation tissue, trafficking of immune cells, resolution of inflammation, drainage of protein-rich lymph from interstitial space, re-establishment of normal tissue pressure, and tissue remodeling during healthy repair [9].

Tooth extractions cause mucosal lacerations and exposure of bone to the oral environment. Consequently, soft tissue and bone interact with each other during the repair process in a unique environment exposed to oral microflora. Once the inflammation subsides, woven bone formation commences from the bottom of the sockets and is associated with an interplay between osteoblasts and osteoclasts [10]. However, lack of socket epithelialization impairs alveolar bone growth, as seen in jaw osteonecrosis [11].

A considerable understanding of the fundamental cellular and molecular mechanisms underlying normal wound healing has been assembled using various mouse models [12]. Reduced lymphatic development as well as disrupted lymphatic function have been shown to impair cutaneous wound healing [13]. Yet, the role of lymphatics during oral wound healing has received less attention. We have previously studied the involvement of lymphatics during periodontal disease development using various transgenic mice models, such as K14-VEGFR3-Ig or K14-VEGFC mice [14, 15]. Genetically engineered K14-VEGFR3-Ig mice have an overexpression of soluble VEGFR3 that competes for VEGF-C/D binding, resulting in the regression of initial lymphatic vessels and lymphedema [16]. The lack of gingival lymphatics in K14-VEGFR3-Ig mice resulted in increased alveolar bone loss and stronger inflammation compared with wild-type (WT) littermate controls after induction of periodontitis by *Porphyromonas gingivalis* challenge [14]. On the other hand, transgenic mice with hyperplastic gingival and oral mucosal lymphatics because of VEGF-C overexpression (K14-VEGFC mice) do not possess an increased drainage capacity and are not protected from bone destruction upon periodontal inflammation [15].

In the light of knowledge gaps on the involvement of lymphatics in the oral wound healing process, we used a tooth extraction model to evaluate how the absence of initial mucosal lymphatics (K14-VEGFR3-Ig mice) or the presence of hyperplastic lymphatics (K14-VEGFC mice) impact mucosal and bone healing.

MATERIAL AND METHODS

Experimental animals

The research protocol comprised details on background, planned sample size, study design, and experimental outcomes; it was approved by the Norwegian Food Safety Authority (FOTS ID 15592) and conducted under supervision of the local Animal Welfare Body at the Laboratory Animal Facility, University of Bergen, Norway. The ARRIVE guidelines were followed in the reporting of the study [17].

Experiments were performed in female transgenic K14-VEGFR3-Ig mice with C57BL/6 background [16] as well as K14-VEGFC mice with FVB background [18], along with corresponding WT controls. Transgenic animals were kindly provided by Dr Kari Alitalo (Molecular/Cancer Biology Laboratory and Haartman Institute, University of Helsinki, Helsinki, Finland). The animals were genotyped by polymerase chain reaction as previously described [15, 19]. We used a total of 104 animals weighing 18–26 g and aged 12–18 weeks. All mice were housed in polycarbonate cages, with no more than five animals per cage. They were fed standard pellet diet with tap water ad libitum. The total number of animals also includes mice that were used in a pilot study to establish procedural standardization and animals that were lost during operations.

Experimental design

Following 7–10 days of acclimatization, the mice were anesthetized i.m. with a total of 0.2 mL mixture of Ketamine 50 mg/mL, administered 100 mg/kg body weight (Ketalar, Pfizer), Xylazine 20 mg/mL, administered 10 mg/kg body weight (Rompun Vet, Bayer) and sodium chloride (NaCl) 9 mg/mL, 0.12 mL/dosage. The animals were then placed on a board to facilitate lower jaw retraction under an operating microscope. The second maxillary molars were extracted with a 23-gauge needle, which was carefully rocked after placement in the mesial, distal, and palatal sulcus. All procedures were performed by one operator. After the extractions, all animals received pain relief medication Buprenorfin (Vetergesic, 0.05 mg/kg body weight, Orion Pharma) and were regularly monitored throughout the various observation periods. The K14-VEGF-C mice and their wild-type WT controls were euthanized at 7- or 14-days post-extraction. The K14-VEGFR-3-Ig animals and their WT controls were observed for either 7, 14, or 21 days.

The maxillae were collected, and randomly number-coded for blinding purposes. One half of each maxilla was used for clinical measurements of the post-extraction wound closure,

European Journal of Oral Sciences NOF Scandinavian Division IADR WILEY

followed by micro-computed tomography and immunohistochemical analyses. The contralateral half of the maxilla was placed in RNAlater (Ambion) and frozen at −80°C until further analysis. Specimens with complete root fractures or bone fractures at the extraction site during tissue handling were excluded from further analyses.

Wound assessment

The jaws were washed with saline for debris and blood remnants detachment. They were placed on a mold which ensured a stable positioning for visualization of the extraction site in line with the remaining first and third molars. A photomicroscope (Nikon Eclipse E600, Nikon) connected to a digital camera employing NIS ELEMENTS AR SOFTWARE (Nikon) was used for visualization, image capturing at 4x magnification and measurement of gross wound closure. The margins of the open wounds were contoured on the captured images, and the areas measured. The results were expressed as squared millimeters and represent averages based on independent evaluations by two investigators (A.V. and L.M.). Interobserver variability was tested (unpaired *t*-test, GRAPHPAD PRISM SOFTWARE VERSION 8, Graphpad). No statistically significant difference in the measurements performed by the two investigators was found. Further analysis was done on averaged values.

After image capture, the jaws were fixed overnight in 4% paraformaldehyde (PFA). They were thereafter washed with 0.1 M phosphate buffer and frozen in phosphate buffer saline at −80°C until further analysis.

Micro-computed tomography (μCT) analysis of bone healing

Briefly, PFA-fixed jaws were placed in a μ-CT scanner with high resolution (Skyscan 1172VR, Bruker). Acquired images were transformed into sliced volumetric reconstruction using NRecon v1.7.1 (Bruker) and down streamed to the molar region by CTAN SOFTWARE V1.18.8 (Bruker). A fixed rectangle shape was loaded onto the dataset, placed within the alveolar socket above the cortical bone and between the first and third molars and 50 layers of images inside each extraction socket were chosen as volume of interest for further analysis. Volume and morphology of the bone within the socket were assessed in three dimensions by thresholding of this region to separate mineralized tissue from the marrow. Outcome parameters of the extraction socket bone included bone volume/tissue volume (BV/TV, %), relative trabecular thickness (Tb.Th/TV, mm/mm^3), relative trabecular separation (Tb.Sp/TV, mm/mm^3), relative trabecular number (Tb.N/TV, 1/mm/mm^3), trabecular pattern factor (Tb.Pf, 1/mm), bone surface density (BS/TV, 1/mm), connectivity density (Conn.Dn, 1/mm^3), structure model index (SMI), previously described by Bouxstein et al. [20]. A 3D analysis and bone mineral density (BMD, g/cm^3) of bone micro-structure in the extraction sockets was also performed by CTAn.

Statistical analyses of wound areas and μCT analysis

The statistical analyses were performed using R VERSION 4.0.3 8R (Development Core Team 2020; http://www.r-project.org) and GRAPHPAD PRISM SOFTWARE VERSION 8 (GraphPad). For analyzing the different response variables, we mainly used two-way ANOVA models allowing for the interaction between the predictors "Animal model" and "Days after treatment" (tooth extraction). Days after treatment were treated as a categorical variable due to the limited resolution in time (7, 14, and 21 days after tooth extraction). For natural reasons, the variance of the response "Wound area" is expected to go down over time. Thus, for this response variable we used a generalized linear model (glm) with log-link function and using a quasi-poisson adjustment of the error term to account for overdispersion. We also analyzed wound area as healed (1) or not healed (0) by using a binary logistic model. For all models indicating an interaction effect between the two predictors "Treatment" and "Days after tooth extraction" or an effect of "Treatment," we did planned comparisons between the two treatment groups for all three levels of "Days after tooth extraction," that is, three planned comparisons. Results are presented as a mean value ± SD. $p < 0.05$ was considered statistically significant.

Immunohistochemical analysis

The PFA-fixed maxillae used for μCT analysis were decalcified in 10% EDTA, washed in phosphate buffer and stored in 30% sucrose at −80° C until cryosectioning. Sections of 14–18 μm thickness were subjected to immunohistochemical analysis for the presence of LYVE-1$^+$ lymphatics, CD31$^+$ blood vessels, F4/80/iNOS$^+$ or CD80$^+$ M1 and Arginase-1$^+$ M2 macrophages and Ly-6.B2+ neutrophils using the avidin-biotin peroxidase (ABC) method and 3,3′-diaminobenzidine (DAB) as the chromogen, as previously described [14, 21]. Briefly, normal rabbit or goat serum (Vector Laboratories) were used for the blocking step, followed by primary antibodies with overnight incubation at 4°C. Antigen-antibody complexes were evidenced by the ABC method, using commercially available kits (Vectastain ABC kit, Vector Laboratories; HRP-DAB cell & tissue staining kit, RnD Systems)

and visualized by 3, 3′-diaminobenzidine (DAB; Sigma-Aldrich). Finally, the sections were counterstained with methylene blue/azure II, dehydrated in graded alcohol series, cleared in xylene and cover slipped with Eukitt (O. Kindler). All sections were visualized under a photomicroscope (Nikon Eclipse E600, Nikon) connected to a digital camera employing LUCIA IMAGING SOFTWARE V.480 (Laboratory Imaging) and representative images were captured. Identification of F4/80/iNOS$^+$ M1 and Arginase-1$^+$ M2 macrophages, as well as simultaneous staining of blood (CD31) and lymphatic vessels (LYVE-1) was performed by use of immunofluorescent double labelling. The antibody-antigen complexes were visualized with Alexa Fluor -488/-546 secondary antibody conjugates (dilution 1:300, Invitrogen). Fluorescent images were captured with a fluorescent microscope (Axio Imager, Carl Zeiss) connected to an AxioCam MRm camera (Carl Zeiss) that used the AXIOVISION 4.8.1 (Carl Zeiss) imaging system. The employed primary antibodies were Ly-6B2 rat anti-mouse, 1:300 (MCA771G, Bio-Rad); F4/80 rat anti-mouse, 1:200 and 1:100/immunofluorescence (ab6640, Abcam); iNOS rabbit anti-mouse, 1:200 (ab3523, Abcam); Arginase-1 rabbit anti-mouse, 1:100 (PA5-29645, Invitrogen); LYVE-1 rabbit anti-mouse 1:300 (ab14917, Abcam) and CD31 goat anti-mouse 1:100 (AF 3628, Bio-Techne).

Analysis of gingival and bone proteins

Buccal, palatal, and interproximal gingiva around the first and third molars, and soft tissue from the extraction site were carefully dissected under an operating microscope. Bone blocks containing the first molar and extraction site were freed from remaining soft tissue and collected separately. All samples were weighed and disrupted in a total volume of 200–500 μL cell lysis buffer (Cell Signaling Technology), supplemented with 1 mM phenylmethanesulfonyl Fluoride (PMSF), Protease Inhibitor Cocktail (Cell Signaling Technology) and gentamicine 10 mg/mL (Sigma-Aldrich). The supernatants were collected after centrifugation and subsequently frozen at −80°C until further analysis.

Protein profiler assay

Protein concentrations were measured using the Pierce Protein Assay Kit (Thermo Fisher Scientific) according to manufacturer's directions. Gingiva or bone samples were pooled for WT or transgenic mice at each observation period. The Mouse XL Cytokine Array Kit (R&D Systems, ARY028) was used for the assessment of relative levels of a total of 111 proteins. The total amount of protein to attain optimal sensitivity was calculated at 200 μg, according to company's instructions. Briefly, after being placed in blocking buffer at room temperature for 1 h, the membranes were incubated with tissue samples overnight at 4°C. Following rinsing with washing buffer three times for 10 min, membranes were incubated with a biotinylated detection antibody cocktail at room temperature for 1 h and then with streptavidin–horseradish peroxidase for 30 min. Membranes were exposed to chemiluminescent detection agents and the signals corresponding to the amount of bound protein measured with the Fujifilm LAS-3000 Luminescent Image Analyzer. Dot spot densities were analyzed using IMAGEJ SOFTWARE (NIH). Loading variability between separate membranes was controlled by densitometry of the positive control spots. The relative expression of each analyte was normalized to the mean density of positive controls (biotinylated IgG).

Multiplex analysis

Following the proteomic profiling of gingiva and bone samples, selected biomarkers were quantitatively evaluated by use of multiplex technology (Multiplex Mouse Discovery Assay LXSAMSM-14, R&D/Bio-Techne; Milliplex MKI2MAG-94K and MAP2MAG-76K, Millipore). These molecules were included in the analyses: C-reactive protein (CRP), serum amyloid P (SAP), lipocalin-2 (LCN2), chitinase-3-like protein 1 (Ch3l1), receptor activator of nuclear factor kappa-B ligand (RANKL), epidermal growth factor (EGF), cystatin C (CST3), insulin like growth factor binding protein 1 (IGFBP1), intercellular adhesion molecule 1 (ICAM1), low density lipoprotein receptor (LDLR), interleukin-33 (IL33), osteopontin (OPN), matrix metalloproteinase 9 (MMP9), chemokine ligand 5 (LIX), periostin (POSTN), chemokine ligands 21 and 22 (CCL21, CCL22). In brief, the samples were diluted (1:2 to 1:320) according to manufacturer's instructions to ensure readouts within the linear range of the standard curve and then incubated with antibody-immobilized beads overnight. Complexes were washed, incubated with biotinylated detection antibody and thereafter, with streptavidin-phycoerythrin. Standard curves for the different analyzed factors were established according to ranges provided by the manufacturers. The levels of molecules were read with a Luminex MAGPX18087721 device and XPONENT ACQUISITION SOFTWARE (Luminex). Final concentrations were calculated corresponding to the standard values and presented as pg or ng biomarker/mg total protein. GRAPHPAD PRISM SOFTWARE, VERSION 8 (GraphPad) was used for representation and statistical analysis of data with two-way ANOVA test method. A list of all evaluated analytes is presented in Table S1.

European Journal of Oral Sciences

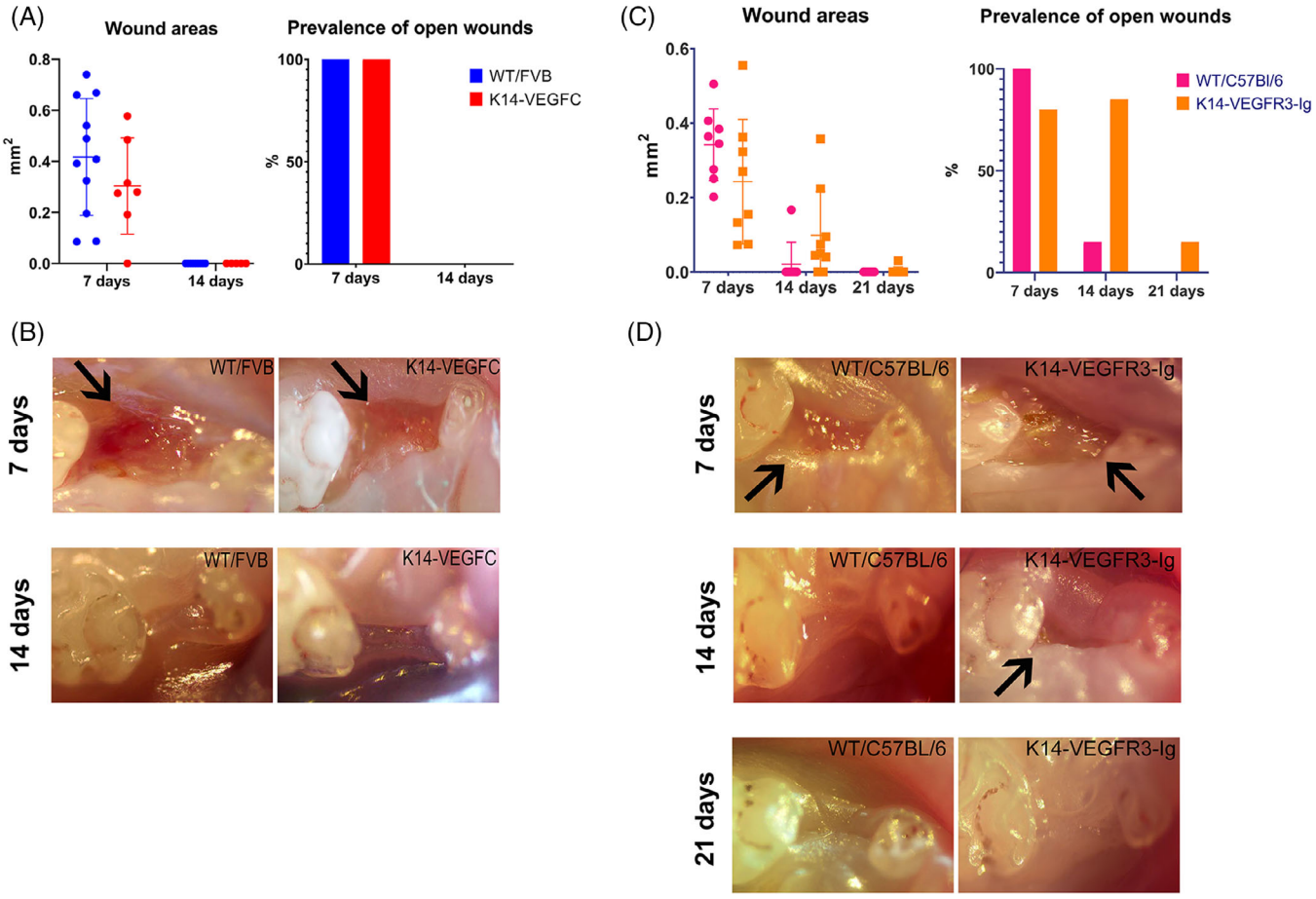

FIGURE 1 Wound areas and exemplification of the clinical appearance at days 7, 14, and 21 post-extraction. A decrease in wound areas (mm^2, mean ± SD) is seen in all investigated groups over the observational periods (A and C). Wound areas of K14-VEGFC mice were not significantly different than their corresponding WT controls (A), whereas all wounds in both phenotypes resulted in closure after 2 weeks observation time (A and B). Wound areas above 0 mm^2 were considered as open. K14-VEGFR3-Ig mice healed slower than WT controls ($p = 0.06$, two-way ANOVA followed by Tukey's multiple comparisons test), resulting in a higher prevalence of open post-extraction wounds at day 14 and day 21 (C). Exemplification of the clinical presentation in WT and transgenic animals at all observation periods (B and D). Open wounds are marked with arrows. ($n = 11$ WT/FVB and $n = 7$ K14-VEGFC 7 days; $n = 6$ WT/FVB and $n = 7$ K14-VEGFC 14 days; $n = 8$ WT/C57Bl/6 and $n = 8$ K14-VEGFR3-Ig 7 days; $n = 8$ WT/C57Bl/6 and $n = 9$ K14-VEGFR3-Ig 14 days; $n = 7$ WT/C57Bl/6 and $n = 8$ K14-VEGFR3-Ig.). WT, wild-type.

RESULTS

Wound closure in transgenic K14-VEGFC and K14-VEGFR3-Ig mice

To assess wound epithelialization following tooth extraction, the areas of open wounds were measured at the different time points. Post-extraction wound areas (mm^2) decreased over time in all mice groups (Figure 1A–D). There was no difference between wound epithelialization of K14-VEGFC and their WT controls (Figure 1A,B). The proportion of open wounds in K14-VEGFR3-Ig animals was higher after 14 and 21 days compared with their littermate controls at equivalent time periods (Figure 1C).

Alveolar bone healing in K14-VEGFC and K14-VEGFR3-Ig mice

Bone filling within the sockets occurred in all groups of mice during the observation periods. No differences were registered between WT and K14-VEGFC mice at bone level on day 7 and day 14 (Figure 2A). Bone volume, relative trabecular bone number, bone surface density and bone mineral density were significantly lower in K14-VEGFR3-Ig compared with WT mice at day 14, indicating delayed bone growth in K14-VEGFR3-Ig transgenic mice. (Figure 2D).

No differences in mucosal and alveolar bone healing between K14-VEGFC and WT littermate controls were noted suggesting that hyperplastic oral mucosal lymphatics, known to characterize this mouse model from current and previous

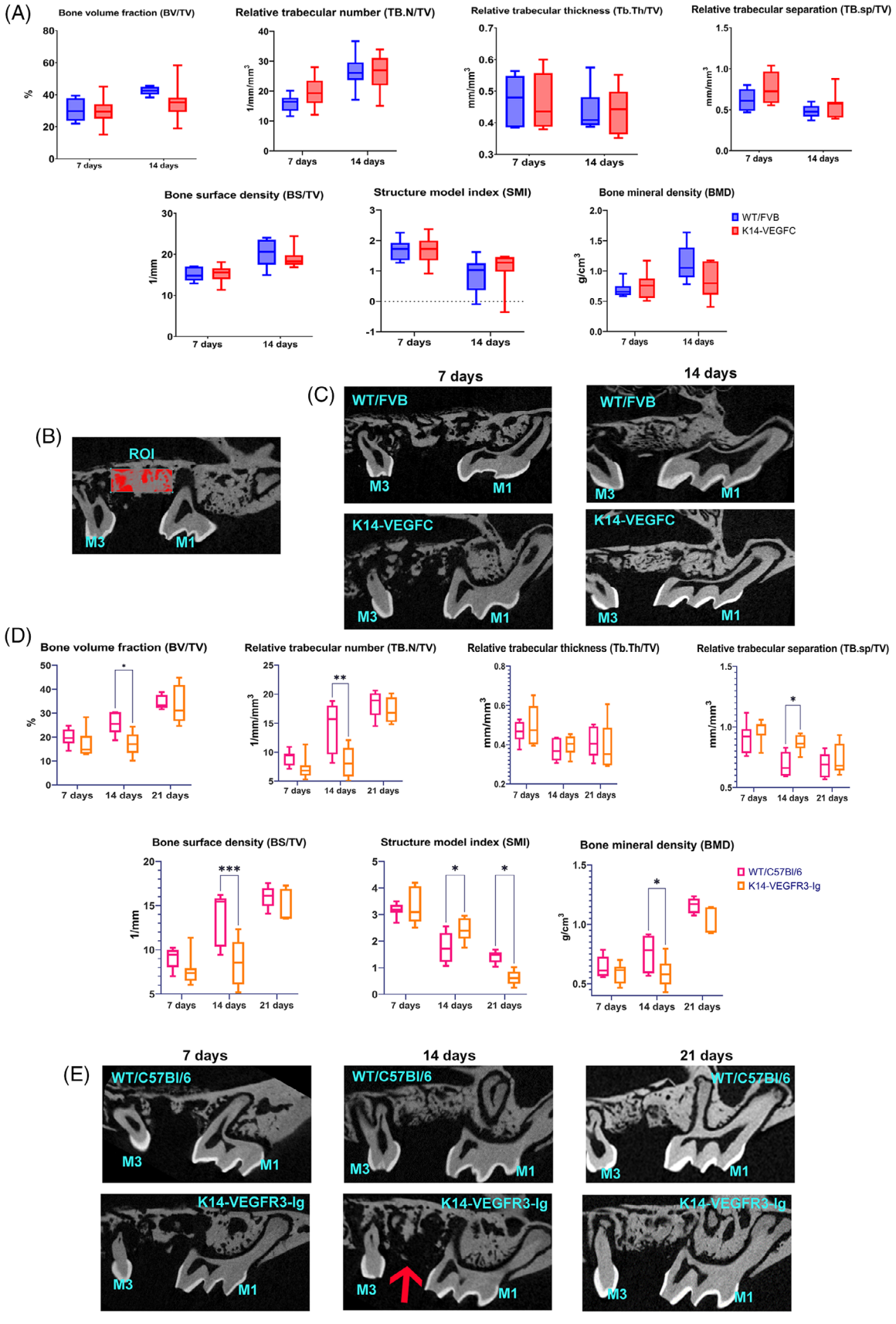

investigations [15], did not enhance the healing process. As such, no further analyses were performed on K14-VEGFC mice and their WT controls.

Neutrophils and M2 macrophages in post-extraction wounds of K14-VEGFR3-Ig mice

As exemplified in Figure 3, we evaluated the presence of different immune cells within the post-extraction wounds by immunohistochemistry. On day 7, a rich inflammatory infiltrate of Ly-6.B2$^+$ neutrophils was present in both K14-VEGFR3-Ig and WT mice. This infiltrate persisted after 2 weeks in alveolar sockets with incomplete epithelialization, and a large infiltrate was found in transgenic mice (Figure 3A). Arg1$^+$ M2 macrophages were abundant after 1 week and only seen in post-extraction wounds, whereas at day 14 they persisted in partially epithelized post-extraction tissue and were nearly absent from epithelized sockets (Figure 3B). Few neutrophils were still present after 21 days (Figure 3A) and Arg1$^+$ macrophages were rarely encountered in healed alveolar socket tissue of both mouse phenotypes (Figure 3B). Exemplification of double immunofluorescent staining of macrophages is presented in Figure S1.

Lymphatic vessels in post-extraction wounds of K14-VEGFC and K14-VEGFR3-Ig mice

Lymphangiogenesis took place during wound healing in both WT controls and in K14-VEGFC mice as was observed as ingrowth of lymphatic vessels underneath the newly formed epithelium (Figure 4A,B). No lymphatic vessels were seen in the post-extraction wounds during the 3-week observation period in the K14-VEGFR3-Ig mice confirming the phenotype used (Figure 4C). CD31$^+$ blood vessels were abundantly present in both mouse phenotypes and WT controls at all observation times (Figure 4B,C).

Evaluation of inflammatory markers in gingiva and bone samples from K14-VEGFR3-Ig mice and WT controls

After observing delayed mucosal and bone healing in K14-VEGFR3-Ig mice, we screened for several proteins (total 111 chemokines, cytokines, growth factors and enzymes) related to biological responses during wound healing. The relative expression of selected markers in both pooled mucosal and pooled bone samples from K14-VEGFR3-Ig and WT mice are presented in Figure 5.

Certain biomarkers discovered during initial screening were further quantitatively evaluated by Multiplex technology. Concentration of acute phase CRP was higher in K14-VEGFR3-Ig than WT controls on day 14. Higher concentrations of gingival chitinase 3 like protein 1 (CHI3L1) and matrix metalloproteinase 9 (MMP9) were registered in transgenic mice samples than in their WT controls after 21 days, although the differences were not statistically significant. Epidermal growth factor (EGF) was lower in transgenic than in WT mice over time, with statistically significantly lower values at bone level after 3 weeks (Figure 6). CCL21 was only expressed in WT gingival samples at all observation times; but expressed in both WT and transgenic bone samples with significantly lower values in K14-VEGFR3-Ig animals, confirming the phenotypes used (Figure 6).

Other biomarkers showed no differences in expression patterns between the two mouse phenotypes (Figure S2). Figure S3 reveals the interactions between all analyzed biomarkers after the initial screening by use of a cytokine array and after their quantitative multiplex analysis (String database, STRING: functional protein association networks (string-db.org).

FIGURE 2 Different parameters of bone healing analysis by μCT (A and D). The parameters were measured within a defined region of interest (red rectangle) between the first and third molar (ROI, B). No significant differences in bone microarchitecture were observed between K14-VEGFC mice and their corresponding controls (A). Panel C illustrates similar bone fill patterns over the 2-week observation period between K14-VEGFC mice and their littermate controls. A significantly faster increase in bone volume ($p = 0.04$) and mineral density ($p = 0.04$), along with number of trabeculae ($p = 0.04$) is seen in WT compared with K14-VEGFR3-Ig animals. The relative trabecular thickness decreased over time and maintained stable values in all groups of mice, with no significant differences between the phenotypes (D). An overall reduction in the relative trabecular separation was also observed, with K14-VEGFR3-Ig mice showing a higher mean value compared to controls, significantly different at 14 days post-extraction- ($p = 0.03$). Bone surface density was significantly different after 2-week observation time ($p = 0.0007$). SMI is indicative of the structure of bone trabeculae, pointing at differences between the two mouse phenotypes, which are significant at 2- and 3-week observation periods ($p = 0.04$); herein, parallel trabeculae result in values closer to 0, while in the case of cylindrical rods the values increase up to 4 (D). The lower panels illustrate bone fill patterns in WT and K14-VEGFR3-Ig mice over the 3-week period (E). A delayed bone fill was noted in K14-VEGFR3-Ig mice after 2 weeks compared to WT controls (arrow). After 3 weeks bone fill occurred similarly in K14-VEGFR3-Ig animals and their controls (D, E). ($n = 6$ WT/FVB and $n = 6$ K14-VEGFC 7 days; $n = 6$ WT/FVB and $n = 7$ K14-VEGFC 14 days; $n = 9$ WT/C57Bl/6 7 and $n = 7$ K14-VEGFR3-Ig 7 days; $n = 5$ WT/C57Bl/6 and $n = 6$ K14-VEGFR3-Ig 14 days; $n = 5$ WT/C57Bl/6 and $n = 5$ K14-VEGFR3-Ig, two-way ANOVA followed by Tukey's, Bonferroni and Sidak's multiple comparisons tests). μCT, micro-computed tomography; SMI, structure model index; WT, wild-type.

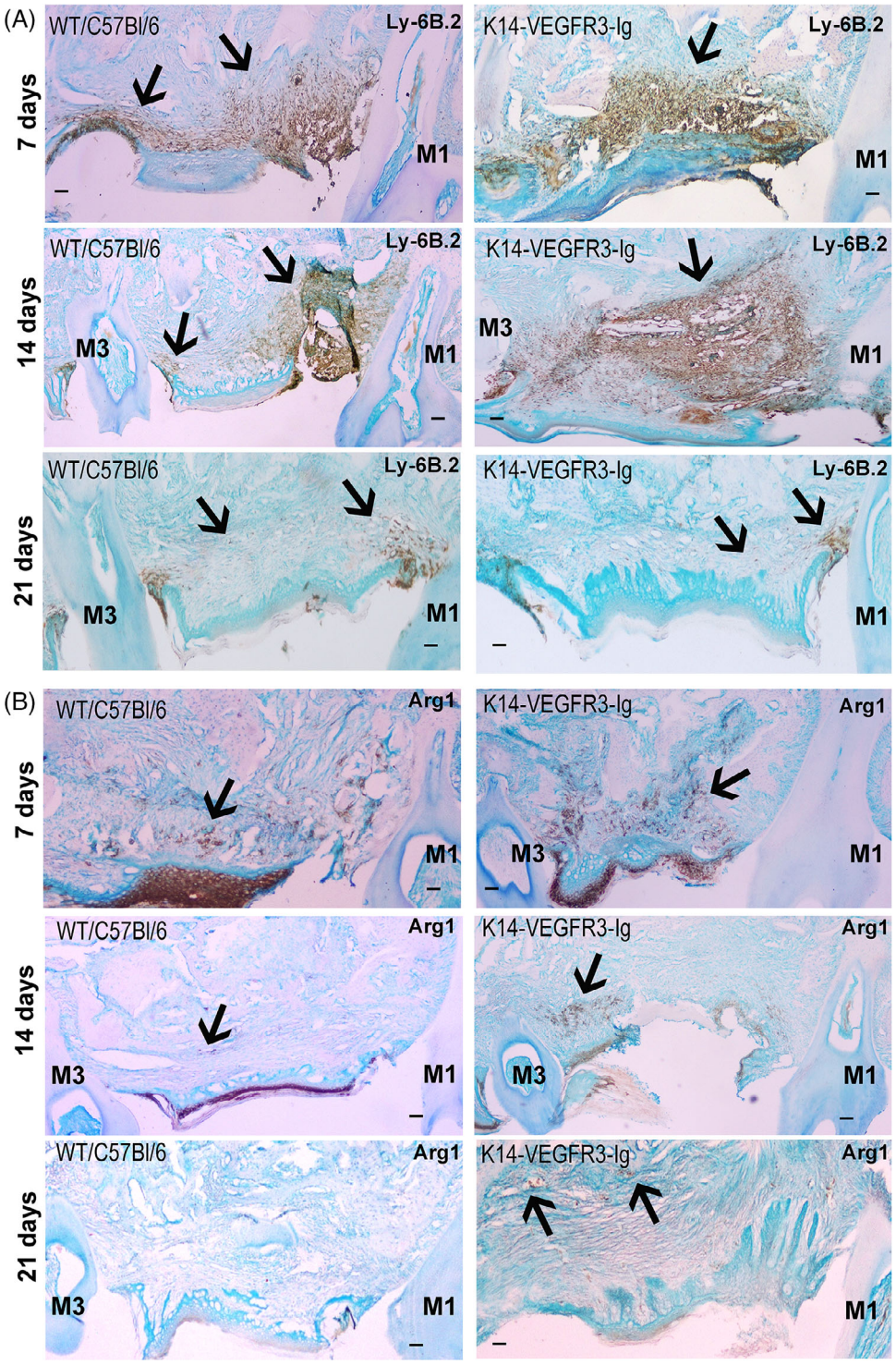

FIGURE 3 Exemplification of cellular infiltrates in post-extraction wounds over the 3-week period. Neutrophil infiltrates (Ly-6.B2$^+$, arrows) are abundant at day 7 in the post-extraction wounds of both mouse phenotypes. By day 14, as healing proceeds, neutrophils persist in non- and partially epithelized areas, with a higher prevalence in transgenic mice. Only few Ly-6.B2$^+$ neutrophils are seen in the newly formed tissue at day 21, and mostly in the sulcus epithelium of neighboring first and third molars (A). Panel B exemplifies the presence of Arg1$^+$ macrophages in the post-extraction wounds. Within the sockets, Arg1$^+$ cells are abundant in non-epithelized wounds up to 2 weeks observation time in both mouse phenotypes, whereas within the healed tissue they are rarely encountered. (Scale bar 10 μm).

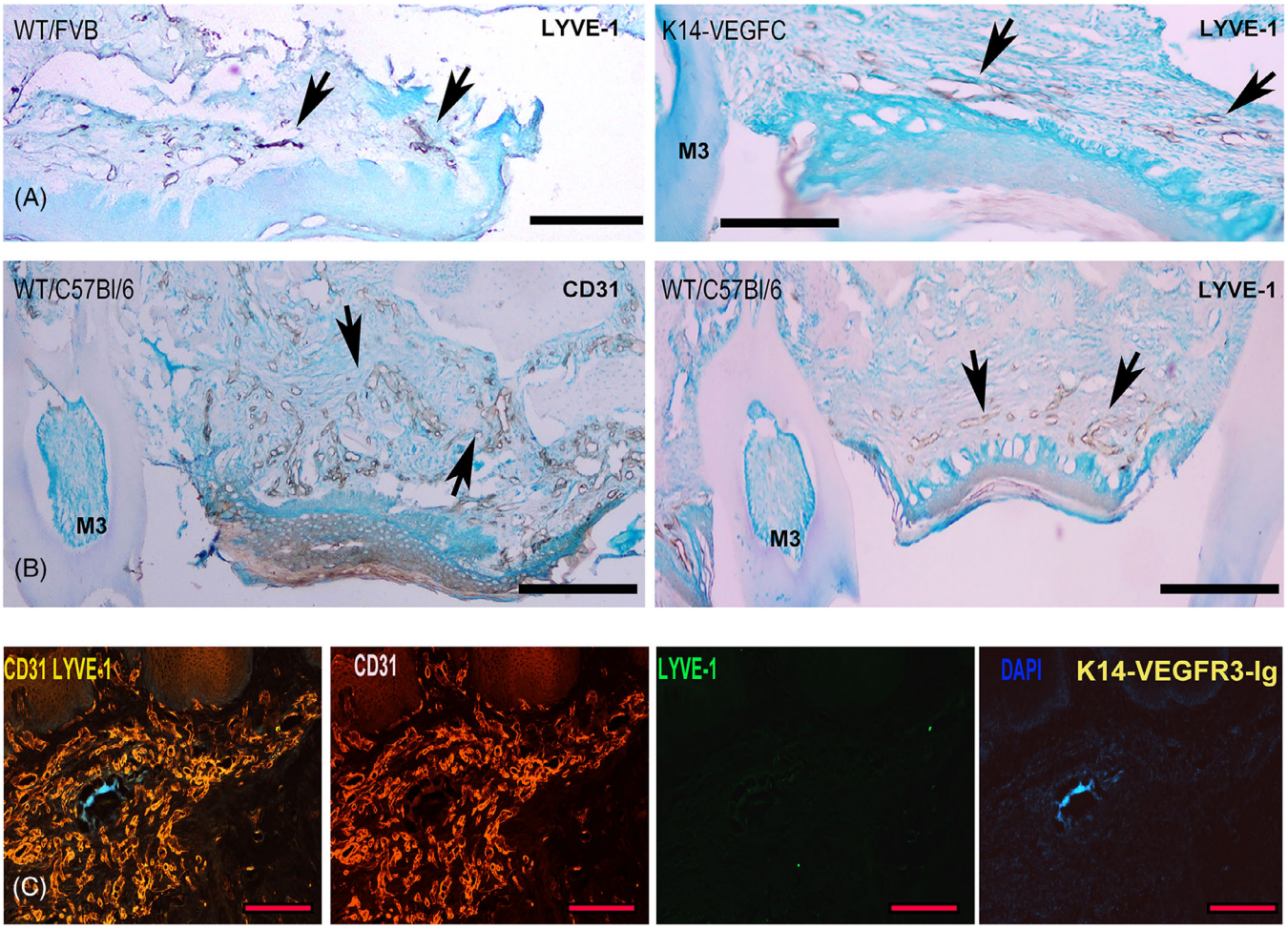

FIGURE 4 Immunohistochemical staining for lymphatic (LYVE-1) and blood (CD31) vessels. Lymphatics were confirmed in sections from K14-VEGFC mice and all WT controls (arrows), here exemplified after one (A) and 2-week observation time (B). Blood vascular structures positive for CD31 (arrows) were found within the jaws and post-extraction alveolar sockets of both mouse phenotypes and their controls at all observation times, here exemplified in panel B on a section from 14 days observation (WT). No lymphatic vessels were seen in the post-extraction wounds of K14-VEGFR3-Ig mice, here confirmed by double immunofluorescent staining in a section from 2 weeks observation time (C). (Scale bar 200 μm). WT, wild-type.

DISCUSSION

The findings of this study have demonstrated that the absence of initial lymphatics in the oral mucosa delays wound healing in a tooth extraction model, manifested as increased prevalence of open wounds after 14- and 21-days post-extraction (Figure 1), along with delayed bone fill of alveolar sockets in the K14-VEGFR3-Ig mice at the 2 weeks observation period (Figure 2). Transgenic mice with hyperplastic mucosal lymphatics (K14-VEGFC) showed no difference in healing patterns of oral mucosa or bone compared with WT controls (Figures 1 and 2).

The lack of initial lymphatics is distinguished at molecular level in K14-VEGFR3-Ig mice by the absence of CCL21 in gingival samples. CCL21 is mainly expressed by the lymphatic endothelium and is required for lymph angiogenesis, a process considered necessary for normal wound healing and inflammatory resolution [13]. In the inflammatory wound environment, increased secretion of CCL21 by lymphatic endothelial cells promotes increased migration of antigen-presenting cells. This helps stimulate the immune response and assists the healing process by removing bacteria and other cellular products from the site [22]. Absence of lymphatics in the post-extraction wounds and on their edges, impairs drainage and clearance processes from the inflammatory site during wound healing, leading to a prolonged inflammatory response in K14-VEGFR3-Ig mice. In addition, a reduced antigen presenting cell mobilization takes place when initial lymphatics are missing. Even though transgenic mice exhibited significantly low levels of CCL21, other factors involved in immune cell recruitment, like chemokines CXCL5 and CCL22, and ICAM1, showed similar expression levels in

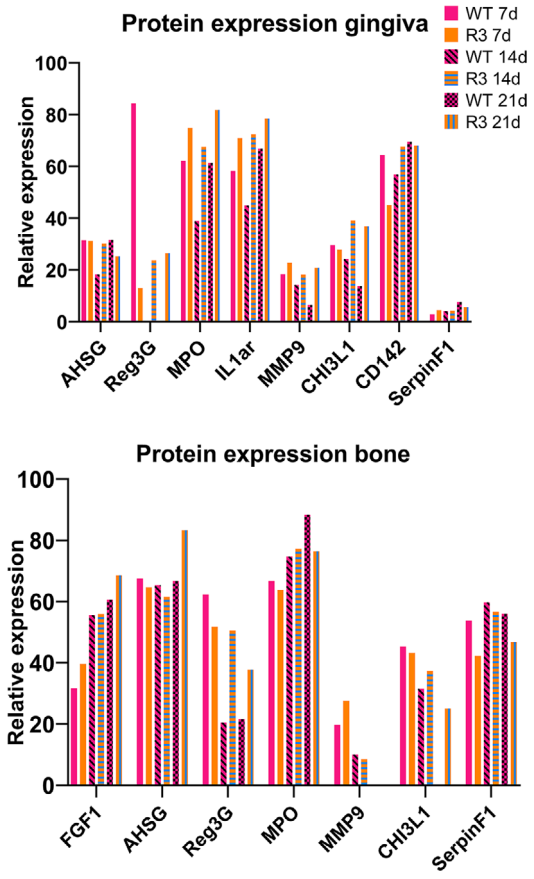

FIGURE 5 An overview of the relative expression of selected proteins investigated in pooled samples of gingiva or bone from all three time periods in WT and K14-VEGFR3-Ig (R3) mice. A higher relative expression of MMP9, CHI3L1, IL1r1, MPO and Reg3G was maintained in gingival samples of K14-VEGFR3-Ig mice after 14 and 21 days. IL1r1 and CD142 were only expressed in gingival samples, whereas FGF1 was only registered in bone samples. A higher relative expression of SerpinF1 and AHSG was noted in bone compared with gingiva samples in both mouse phenotypes over time. WT, wild-type.

mucosal and bone samples as seen in WT controls (Figure S2).

The findings confirmed the presence of rich blood vascular structures and immune cells within the alveolar sockets of both K14-VEGFR3-Ig mice and their littermates during the 3-week observation period. Furthermore, K14-VEGFR3-Ig mice present with lymphatics in the deeper layers of the alveolar mucosa [14]. The role of chemokines such as CXCL5, CCL22 and ICAM1 in angiogenesis is well-established [23]. We therefore assume that lymphatic vessels present at submucosal levels, along with blood vessels, are sufficient for normal immune cell trafficking in K14-VEGFR3-Ig mice.

In the current study, abundant infiltrates of neutrophils and macrophages persisted in the post-extraction wounds of mice with no or partially epithelized sockets. In addition, only few differences were seen in biomarker levels between WT and K14-VEGFR3-Ig mice. EGF expression was significantly lower in mucosal and bone samples in K14-VEGFR3-Ig compared to WT mice. EGF influences keratinocyte migration that determines the speed of wound epithelialization [24]. Keratinocytes are the executors of the re-epithelialization process, whereby they migrate, proliferate, and differentiate to restore the epidermal barrier [24]. Previous investigations have linked skin lymph angiogenesis during wound healing to activation of EGF [25]. Furthermore, gingival epithelial cells may produce angiogenic and lymphangiogenic factors upon inflammatory insults and stimulate vessel formation [26]. In the absence of initial lymphatics in K14-VEGFR3-Ig mice, concomitant with low expression of EGF, we found delayed post-extraction epithelialization. In addition, we have shown a hampered bone growth and mineralization in the same mouse phenotype. EGFR signaling plays an important role in bone remodeling by affecting both bone formation and resorption, during healing [27, 28]. Significantly lower levels of EGF were measured in the bone and this finding may also explain the delayed alveolar bone healing. However, epithelial and bone healing did occur in both mouse phenotypes after 21 days, indicative that K14-VEGFR3-Ig mice maintain their healing capacity after tooth extraction.

Open chronic wounds correlate with a prolonged inflammatory phase during wound healing [29]. In the current study, non-epithelialized wounds were more prevalent 14 days post-extraction in K14-VEGFR3-IG mice, with abundant infiltrates of neutrophils and macrophages that contribute to the production of inflammatory mediators. Pro-inflammatory markers such as CRP and MPO maintained elevated mucosal levels after 2-week observation time, pointing again at an extended inflammatory response in K14-VEGFR3-Ig animals. CRP can be synthetized locally, even in the gingiva [30] by macrophages and endothelial cells [31]. MPO, an antibacterial molecule with neutrophils as primary source, may result in collateral tissue damage and decrease the speed of wound repair [32].

CHI3L1 plays an important role in tissue repair, angiogenic responses and M2 macrophage differentiation, with both pro- and anti-inflammatory effects [33, 34]. MMP9 also has a dual role during wound healing, with reports of both accelerated and delayed closure in the event of abundant MMP9 expression [35], along with being essential to healing after bone fracture [36]. Even though not statistically significant, their levels remained elevated in transgenic mice compared with WT controls at day 21. The lack of statistical significance may be attributed to the relatively small sample size which was included in the protein analysis. Since epithelialization and bone fill occurred in both mouse phenotypes, we assume that CHI3L1 and MMP9 contribute to the healing process during proliferation and remodeling stages of oral wound repair.

It has been shown that anti-inflammatory cytokines in both healing and non-healing diabetic wounds are mainly produced by macrophages [37]. The local environment determines

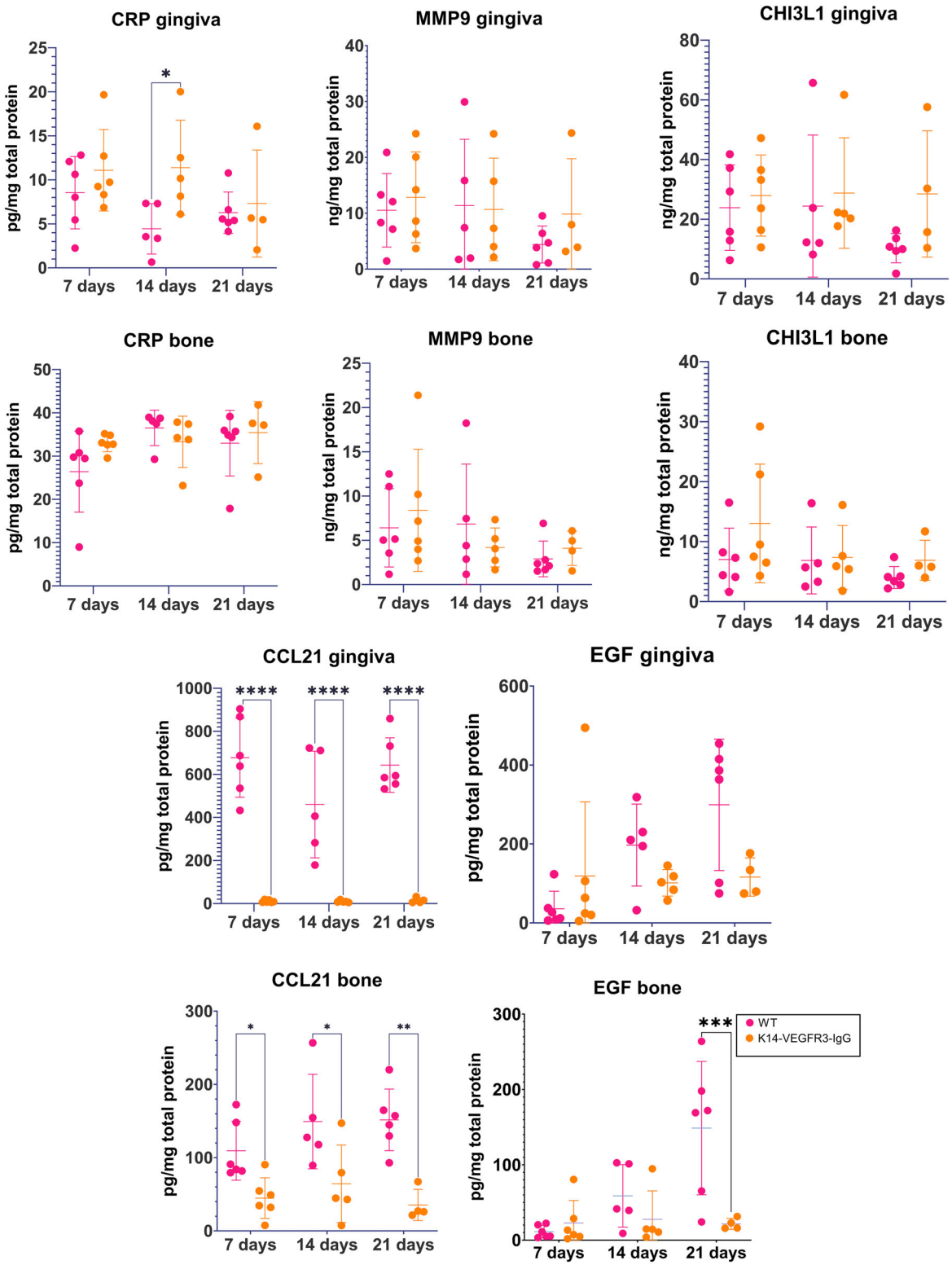

FIGURE 6 Quantitative expression of various growth factors, enzymes, cytokines and chemokines from each sample and observation period. CRP levels were significantly increased after 14 days in transgenic gingival samples compared with their controls ($p = 0.04$). Higher values, yet not statistically significant of gingival CH3L1 and MMP9, were found in K14-VEGFR3-Ig mice after 21 days compared with WT animals. Transgenic mice did not express CCL21 in the gingiva, while this chemokine maintained significantly lower levels within the bone samples of K14-VEGFR3-Ig animals ($p < 0.04$). EGF expression was higher in WT samples after 14 and 21 days in both gingiva and bone, significant for the latter at the 3 weeks period only ($p = 0.0008$). ($n = 6$ WT/C57Bl/6 7 and $n = 6$ K14-VEGFR3-Ig 7 days; $n = 5$ WT/C57Bl/6 and $n = 5$ K14-VEGFR3-Ig 14 days; $n = 6$ WT/C57Bl/6 and $n = 4$ K14-VEGFR3-Ig, two-way ANOVA followed by Sidak's multiple comparisons tests). CRP, C-reactive protein; EGF, epidermal growth factor; WT, wild-type.

macrophage differentiation into pro-inflammatory (M1) or anti-inflammatory (M2) cells, with multiple cytokines being able to interchange macrophage plasticity [38]. Both iNOS$^+$ M1 and Arg1$^+$ M2 macrophages were present in the wounds of both mouse phenotypes. Yet, at day 14, Arg1$^+$ macrophages were predominant in non- or partially epithelialized wounds, indicating the start of inflammatory resolution and tissue repair.

There was a delayed bone fill, along with a reduced mineral density of newly formed bone of K14-VEGFR3-Ig mice. Animal studies have shown that bone formation begins during the proliferative phase [39], which in this transgenic model is delayed due to extended inflammation. Nevertheless, at molecular level, there were no different expression patterns for bone activity markers such as RANKL, PSTN or OPN between the two phenotypes, showing that K14-VEGFR3-Ig mice maintain their capacity of bone deposition.

After induction of periodontal disease, K14-VEGFC animals did not show any differences when compared with WT animals in terms of bone resorption [15]. In the current study, K14-VEGFC mice had similar bone healing patterns as their WT littermates. Even though lymphatics are considered essential to skin and mucosal wound healing, increased areas of hyperplastic gingival lymphatics, as seen in K14-VEGFC mice, did not influence bone growth or accelerate post-extraction wound healing. In a recent paper, lymphatic vessels were identified in long bones in mice, and lymphatic endothelial cells were shown to be responsible for signaling osteoblasts during bone regeneration via CXCL12 [40].

A potential limitation of the study is the use of two different background strains: transgenic K14-VEGFR3-Ig mice with C57BL/6 background as well as K14-VEGFC mice with FVB background. The different background of the strains did, however, not affect our conclusions because no direct comparisons were made between the transgenic animals.

Translating our findings to a clinical perspective, this study indicates that delayed oral wound healing associates with a persistent inflammation of the oral mucosa in areas devoid of lymphatics. Screening for an ideal biomarker to evaluate wound healing is difficult due to the pleiotropic role of cytokines in physiology and disease. Exploring these networks in the future can lead to new research opportunities of oral conditions and possibly therapeutic approaches to promote wound healing.

In summary, this study has shown that: (i) epithelialization and bone fill of the alveolar sockets are delayed in mice lacking initial mucosal lymphatics (K14-VEGFR3-Ig mice) and are followed by persistent inflammation in post-extraction wounds during the initial phases of the healing process; (ii) the lack of initial lymphatics correlates with low concentrations of EGF from post-extraction wounds and hampered wound closure suggesting an important role of lymphatics during oral wound healing; (iii) increased lymphatic vessel density (hyperplasia) as seen in K14-VEGFC mice, does not influence the wound healing process.

AUTHOR CONTRIBUTIONS

Conceptualization: Anca Virtej, Marek Wagner, Helge Wiig, Ying Xue, Athanasia Bletsa, Ellen Berggreen; **Methodology**: Anca Virtej, Larissa Marti, Marek Wagner, Ying Xue, Athanasia Bletsa, Ellen Berggreen; **Validation**: Anca Virtej, Larissa Marti, Marek Wagner, Ying Xue, Helge Wiig, Athanasia Bletsa, Ellen Berggreen; **Formal analysis**: Anca Virtej, Larissa Marti, Marek Wagner, Ying Xue; **Investigation**: Anca Virtej, Larissa Marti, Marek Wagner, Ying Xue; **Resources**: Anca Virtej, Ying Xue, Helge Wiig; **Data curation**: Ellen Berggreen; **Writing—original draft preparation**: Anca Virtej, Athanasia Bletsa, Ellen Berggreen; **Writing—review and editing**: Anca Virtej, Larissa Marti, Marek Wagner, Ying Xue, Helge Wiig, Athanasia Bletsa, Ellen Berggreen; **Visualization**: Anca Virtej; **Supervision**: Anca Virtej, Ellen Berggreen; **Project administration**: Anca Virtej, Ellen Berggreen; **Funding acquisition**: Anca Virtej, Ellen Berggreen.

ACKNOWLEDGMENTS

We thank Trude Skogstrand for valuable help with genotyping the animals; Hallvard Haugen for assistance with Multiplex analyses and Knut Helge Jensen for support with statistical analyses. Funded by HelseVest project number HV F-11508 and University of Bergen. All authors gave their final approval and agreed to be accountable for all aspects of the work.

CONFLICT OF INTEREST STATEMENT

The authors declare no conflicts of interests.

ORCID

Anca Virtej https://orcid.org/0000-0001-5918-3663
Larissa Marti https://orcid.org/0009-0001-7811-154X
Marek Wagner https://orcid.org/0000-0003-3967-9527
Helge Wiig https://orcid.org/0000-0002-7740-8210
Ying Xue https://orcid.org/0000-0002-2266-3839
Athanasia Bletsa https://orcid.org/0000-0003-2427-8165
Ellen Berggreen https://orcid.org/0000-0001-6077-943X

REFERENCES

1. Eming SA, Martin P, Tomic-Canic M. Wound repair and regeneration: mechanisms, signaling, and translation. Sci Transl Med. 2014;6:265sr6. https://doi.org/10.1126/scitranslmed.3009337
2. Sato H, Takeda Y. Proliferative activity, apoptosis, and histogenesis in the early stages of rat tooth extraction wound healing. Cells Tissues Organs. 2007;186:104-11.
3. Kolaczkowska E, Kubes P. Neutrophil recruitment and function in health and inflammation. Nat Rev Immunol. 2013;13:159-75.

4. Politis C, Schoenaers J, Jacobs R, Agbaje JO. Wound healing problems in the mouth. Front Physiol. 2016;7:507. https://doi.org/10.3389/fphys.2016.00507
5. Mantovani A, Biswas SK, Galdiero MR, Sica A, Locati M. Macrophage plasticity and polarization in tissue repair and remodelling. J Pathol. 2013;229:176-85.
6. Gurtner GC, Werner S, Barrandon Y, Longaker MT. Wound repair and regeneration. Nature. 2008;453:314-21.
7. Baum CL, Arpey CJ. Normal cutaneous wound healing: clinical correlation with cellular and molecular events. Dermatol Surg. 2005;31(6):674-86; discussion 86. https://doi.org/10.1111/j.1524-4725.2005.31612
8. Beerens M, Aranguren XL, Hendrickx B, Dheedene W, Dresselaers T, Himmelreich U, et al. Multipotent adult progenitor cells support lymphatic regeneration at multiple anatomical levels during wound healing and lymphedema. Sci Rep. 2018;8:3852. https://doi.org/10.1038/s41598-018-21610-8
9. Guc E, Briquez PS, Foretay D, Fankhauser MA, Hubbell JA, Kilarski WW, et al. Local induction of lymphangiogenesis with engineered fibrin-binding VEGF-C promotes wound healing by increasing immune cell trafficking and matrix remodeling. Biomaterials. 2017;131:160–75.
10. Cardaropoli G, Araujo M, Lindhe J. Dynamics of bone tissue formation in tooth extraction sites. An experimental study in dogs. J Clin Periodontol. 2003;30:809–18.
11. Landesberg R, Cozin M, Cremers S, Woo V, Kousteni S, Sinha S, et al. Inhibition of oral mucosal cell wound healing by bisphosphonates. J Oral Maxillofac Surg. 2008;66:839–47.
12. Martin P, Nunan R. Cellular and molecular mechanisms of repair in acute and chronic wound healing. Br J Dermatol. 2015;173:370–8.
13. Kimura T, Sugaya M, Blauvelt A, Okochi H, Sato S. Delayed wound healing due to increased interleukin-10 expression in mice with lymphatic dysfunction. J Leukoc Biol. 2013;94:137–45.
14. Mkonyi LE, Bletsa A, Bolstad AI, Bakken V, Wiig H, Berggreen E. Gingival lymphatic drainage protects against Porphyromonas gingivalis-induced bone loss in mice. Am J Pathol. 2012;181:907–16.
15. Papadakou P, Bletsa A, Yassin MA, Karlsen TV, Wiig H, Berggreen E. Role of hyperplasia of gingival lymphatics in periodontal inflammation. J Dent Res. 2017;96:467–76.
16. Makinen T, Jussila L, Veikkola T, Karpanen T, Kettunen MI, Pulkkanen KJ, et al. Inhibition of lymphangiogenesis with resulting lymphedema in transgenic mice expressing soluble VEGF receptor-3. Nat Med. 2001;7:199–205.
17. Kilkenny C, Browne WJ, Cuthill IC, Emerson M, Altman DG. Improving bioscience research reporting: the ARRIVE guidelines for reporting animal research. PLoS Biol. 2010;8(6):e1000412. https://doi.org/10.1371/journal.pbio.1000412
18. Jeltsch M, Kaipainen A, Joukov V, Meng X, Lakso M, Rauvala H, et al. Hyperplasia of lymphatic vessels in VEGF-C transgenic mice. Science. 1997;276:1423–5.
19. Mkonyi LE, Bletsa A, Fristad I, Wiig H, Berggreen E. Importance of lymph vessels in the transcapillary fluid balance in the gingiva studied in a transgenic mouse model. Am J Physiol Heart Circ Physiol. 2010;299:H275–83.
20. Bouxsein ML, Boyd SK, Christiansen BA, Guldberg RE, Jepsen KJ, Muller R. Guidelines for assessment of bone microstructure in rodents using micro-computed tomography. J Bone Miner Res. 2010;25:1468–86.
21. Virtej A, Papadakou P, Sasaki H, Bletsa A, Berggreen E. VEGFR-2 reduces while combined VEGFR-2 and -3 signaling increases inflammation in apical periodontitis. J Oral Microbiol. 2016;8:907. https://doi.org/10.1016/j.ajpath.2012.05.027
22. Johnson LA, Jackson DG. Inflammation-induced secretion of CCL21 in lymphatic endothelium is a key regulator of integrin-mediated dendritic cell transmigration. Int Immunol. 2010;22:839–49.
23. Belperio JA, Keane MP, Arenberg DA, Addison CL, Ehlert JE, Burdick MD, et al. CXC chemokines in angiogenesis. J Leukoc Biol. 2000;68:1–8.
24. Haase I, Evans R, Pofahl R, W FMJJocs. Regulation of keratinocyte shape, migration and wound epithelialization by IGF-1-and EGF-dependent signalling pathways. J Cell Sci. 2003;116:3227–38.
25. Marino D, Angehrn Y, Klein S, Riccardi S, Baenziger-Tobler N, Otto VI, et al. Activation of the epidermal growth factor receptor promotes lymphangiogenesis in the skin. J Dermatol Sci. 2013;71:184–94.
26. Indrelid SH, Dongre HN, Nunes IP, Virtej A, Bletsa A, Berggreen E. Human gingival epithelial cells stimulate proliferation, migration, and tube formation of lymphatic endothelial cells in vitro. J Periodontal Res. 2023;58:596–606.
27. Zhang X, Tamasi J, Lu X, Zhu J, Chen H, Tian X, et al. Epidermal growth factor receptor plays an anabolic role in bone metabolism in vivo. J Bone Miner Res. 2011;26:1022–34.
28. Zhu J, Shimizu E, Zhang X, Partridge NC, Qin L. EGFR signaling suppresses osteoblast differentiation and inhibits expression of master osteoblastic transcription factors Runx2 and Osterix. J Cell Biochem. 2011;112:1749–60.
29. Blakytny R, Jude E. The molecular biology of chronic wounds and delayed healing in diabetes. Diabet Med. 2006;23:594–608.
30. Lu Q, Jin L. Human gingiva is another site of C-reactive protein formation. J Clin Periodontol. 2010;37:789–96.
31. Venugopal SK, Devaraj S, Jialal I. Macrophage conditioned medium induces the expression of C-reactive protein in human aortic endothelial cells: potential for paracrine/autocrine effects. Am J Pathol. 2005;166:1265–71.
32. Slater TW, Finkielsztein A, Mascarenhas LA, Mehl LC, Butin-Israeli V, Sumagin R. Neutrophil microparticles deliver active myeloperoxidase to injured mucosa to inhibit epithelial wound healing. J Immunol. 2017;198:2886–97.
33. He CH, Lee CG, Dela Cruz CS, Lee CM, Zhou Y, Ahangari F, et al. Chitinase 3-like 1 regulates cellular and tissue responses via IL-13 receptor α2. Cell Rep. 2013;4:830–41.
34. Xu N, Bo Q, Shao R, Liang J, Zhai Y, Yang S, et al. Chitinase-3-like-1 promotes M2 macrophage differentiation and induces choroidal neovascularization in neovascular age-related macular degeneration. Invest Ophthalmol Vis Sci. 2019;60:4596–605.
35. Rayment EA, Upton Z, Shooter GK. Increased matrix metalloproteinase-9 (MMP-9) activity observed in chronic wound fluid is related to the clinical severity of the ulcer. Br J Dermatol. 2008;158:951–61.
36. Colnot C, Thompson Z, Miclau T, Werb Z, Helms JA. Altered fracture repair in the absence of MMP9. Development. 2003;130:4123–33.

37. Mirza RE, Koh TJ. Contributions of cell subsets to cytokine production during normal and impaired wound healing. Cytokine. 2015;71:409–12.
38. Davis MJ, Tsang TM, Qiu Y, Dayrit JK, Freij JB, Huffnagle GB, et al. Macrophage M1/M2 polarization dynamically adapts to changes in cytokine microenvironments in Cryptococcus neoformans infection. mBio. 2013;4:e00264–313.
39. Trombelli L, Farina R, Marzola A, Bozzi L, Liljenberg B, Lindhe J. Modeling and remodeling of human extraction sockets. J Clin Periodontol. 2008;35:630–9.
40. Biswas L, Chen J, De Angelis J, Singh A, Owen-Woods C, Ding Z, et al. Lymphatic vessels in bone support regeneration after injury. Cell. 2023;186:382–97.e24

SUPPORTING INFORMATION

Additional supporting information can be found online in the Supporting Information section at the end of this article.

How to cite this article: Virtej A, Marti L, Wagner M, Wiig H, Xue Y, Bletsa A, et al. Contribution of initial lymphatics to oral wound healing after tooth extraction. Eur J Oral Sci. 2024;132:e13006. https://doi.org/10.1111/eos.13006